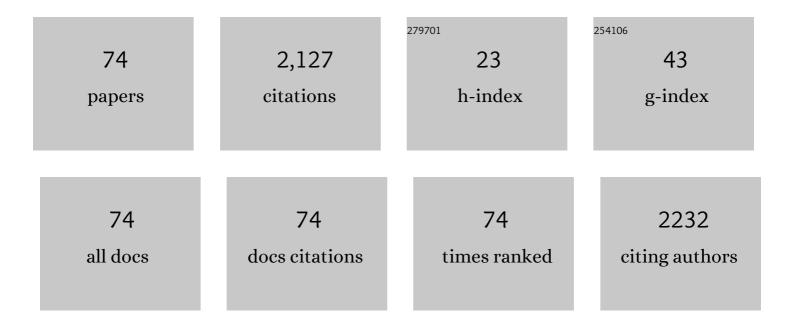
List of Publications by Year in descending order

Source: https://exaly.com/author-pdf/4763683/publications.pdf Version: 2024-02-01



Ορετά Ολεοκιι

#	Article	IF	CITATIONS
1	Soil pore network response to freeze-thaw cycles in permafrost aggregates. Geoderma, 2022, 411, 115674.	2.3	30
2	Enhanced Transport of TiO ₂ in Unsaturated Sand and Soil after Release from Biodegradable Plastic during Composting. Environmental Science & Technology, 2022, 56, 2398-2406.	4.6	6
3	Deciphering the Distribution and Crystal-Chemical Environment of Arsenic, Lead, Silica, Phosphorus, Tin, and Zinc in a Porous Ferrihydrite Grain Using Transmission Electron Microscopy and Atom Probe Tomography. ACS Earth and Space Chemistry, 2022, 6, 558-570.	1.2	4
4	Fungal hyphae develop where titanomagnetite inclusions reach the surface of basalt grains. Scientific Reports, 2022, 12, 3407.	1.6	3
5	Elemental iron: reduction of pertechnetate in the presence of silica and periodicity of precipitated nano-structures. Environmental Science: Nano, 2021, 8, 97-109.	2.2	2
6	Microbe-Encapsulated Silica Gel Biosorbents for Selective Extraction of Scandium from Coal Byproducts. Environmental Science & Technology, 2021, 55, 6320-6328.	4.6	12
7	Deciphering the Incipient Phases of Ice–Mineral Interactions as a Precursor of Physical Weathering. ACS Earth and Space Chemistry, 2021, 5, 1233-1241.	1.2	5
8	Characterizing the localization of organic C on mineral surfaces: a correlative microscopy/spectroscopy approach. Microscopy and Microanalysis, 2021, 27, 306-307.	0.2	0
9	Synergistic Coupling of CO ₂ and H ₂ O during Expansion of Clays in Supercritical CO ₂ –CH ₄ Fluid Mixtures. Environmental Science & Technology, 2021, 55, 11192-11203.	4.6	3
10	Simultaneous immobilization of aqueous co-contaminants using a bismuth layered material. Journal of Environmental Radioactivity, 2021, 237, 106711.	0.9	5
11	Cluster defects in gibbsite nanoplates grown at acidic to neutral pH. Nanoscale, 2021, 13, 17373-17385.	2.8	5
12	Atomic Force Microscopy and Infrared Nanospectroscopy of COVID-19 Spike Protein for the Quantification of Adhesion to Common Surfaces. Langmuir, 2021, 37, 12089-12097.	1.6	5
13	Ion–ion interactions enhance aluminum solubility in alkaline suspensions of nano-gibbsite (α-Al(OH) ₃) with sodium nitrite/nitrate. Physical Chemistry Chemical Physics, 2020, 22, 4368-4378.	1.3	19
14	Evaluation of materials for iodine and technetium immobilization through sorption and redox-driven processes. Science of the Total Environment, 2020, 716, 136167.	3.9	16
15	Labile Fe(III) from sorbed Fe(II) oxidation is the key intermediate in Fe(II)-catalyzed ferrihydrite transformation. Geochimica Et Cosmochimica Acta, 2020, 272, 105-120.	1.6	72
16	Waterâ€dispersible nanocolloids and higher temperatures promote the release of carbon from riparian soil. Vadose Zone Journal, 2020, 19, e20077.	1.3	2
17	Radiation-Induced Interfacial Hydroxyl Transformation on Boehmite and Gibbsite Basal Surfaces. Journal of Physical Chemistry C, 2020, 124, 22185-22191.	1.5	8
18	Low temperature and limited water activity reveal a pathway to magnesite <i>via</i> amorphous magnesium carbonate. Chemical Communications, 2020, 56, 12154-12157.	2.2	17

#	Article	IF	CITATIONS
19	Nanoscale observations of Fe(<scp>ii</scp>)-induced ferrihydrite transformation. Environmental Science: Nano, 2020, 7, 2953-2967.	2.2	21
20	Macro to Nanoscale Approaches to Study Mineral Transformations at the Liquid, Organic, Biological Interface Microscopy and Microanalysis, 2020, 26, 1568-1569.	0.2	0
21	Utilizing Correlative Imaging Approaches with ToF-SIMS Expands Our Biochemical Interpretation Abilities Across Biological Kingdoms. Microscopy and Microanalysis, 2020, 26, 2508-2508.	0.2	0
22	Critical Water Coverage during Forsterite Carbonation in Thin Water Films: Activating Dissolution and Mass Transport. Environmental Science & amp; Technology, 2020, 54, 6888-6899.	4.6	22
23	Hybrid Sorbents for ¹²⁹ I Capture from Contaminated Groundwater. ACS Applied Materials & Interfaces, 2020, 12, 26113-26126.	4.0	19
24	A Correlative Bimodal Surface Imaging Method to Assess Hyphae-Rock Interactions Microscopy and Microanalysis, 2019, 25, 2436-2437.	0.2	3
25	Mineral Surface Transformations by Ice Nucleation. Microscopy and Microanalysis, 2019, 25, 2464-2465.	0.2	Ο
26	Facet-Specific Photocatalytic Degradation of Organics by Heterogeneous Fenton Chemistry on Hematite Nanoparticles. Environmental Science & Technology, 2019, 53, 10197-10207.	4.6	101
27	Association of Defects and Zinc in Hematite. Environmental Science & Technology, 2019, 53, 13687-13694.	4.6	20
28	Role of Fe(II) Content in Olivine Carbonation in Wet Supercritical CO ₂ . Environmental Science and Technology Letters, 2019, 6, 592-599.	3.9	18
29	Can mineral growth by oriented attachment lead to incorporation of uranium(vi) into the structure of goethite?. Environmental Science: Nano, 2019, 6, 3000-3009.	2.2	10
30	Surface-Catalyzed Oxygen Exchange during Mineral Carbonation in Nanoscale Water Films. Journal of Physical Chemistry C, 2019, 123, 12871-12885.	1.5	21
31	A coupled microscopy approach to assess the nano-landscape of weathering. Scientific Reports, 2019, 9, 5377.	1.6	25
32	Synthesis of nanometer-sized fayalite and magnesium-iron(II) mixture olivines. Journal of Colloid and Interface Science, 2018, 515, 129-138.	5.0	19
33	Element mobilization and immobilization from carbonate rocks between CO2 storage reservoirs and the overlying aquifers during a potential CO2 leakage. Chemosphere, 2018, 197, 399-410.	4.2	16
34	The effect of ion irradiation on the dissolution of UO2 and UO2-based simulant fuel. Journal of Alloys and Compounds, 2018, 735, 1350-1356.	2.8	12
35	Technetium and iodine aqueous species immobilization and transformations in the presence of strong reductants and calcite-forming solutions: Remedial action implications. Science of the Total Environment, 2018, 636, 588-595.	3.9	17
36	Bacterial Productivity in a Ferrocyanide-Contaminated Aquifer at a Nuclear Waste Site. Water (Switzerland), 2018, 10, 1072.	1.2	4

#	Article	IF	CITATIONS
37	Characterizing Technetium in Subsurface Sediments for Contaminant Remediation. ACS Earth and Space Chemistry, 2018, 2, 1145-1160.	1.2	8
38	Water Structure Controls Carbonic Acid Formation in Adsorbed Water Films. Journal of Physical Chemistry Letters, 2018, 9, 4988-4994.	2.1	16
39	Trace Uranium Partitioning in a Multiphase Nano-FeOOH System. Environmental Science & Technology, 2017, 51, 4970-4977.	4.6	44
40	Manganese-calcium intermixing facilitates heteroepitaxial growth at the <mml:math xmlns:mml="http://www.w3.org/1998/Math/MathML" altimg="si3.gif" overflow="scroll"><mml:mfenced open="(" close=")"><mml:mrow><mml:mn>10</mml:mn><mml:mover accent="false"><mml:mn>1</mml:mn><mml:mo>Â⁻</mml:mo><mml:mn>4</mml:mn>calcite-water interface. Chemical Geology, 2017, 470, 152-163.</mml:mover </mml:mrow></mml:mfenced </mml:math 	1.4 w> <td>17 nfenced></td>	17 nfenced>
41	Tc(VII) and Cr(VI) Interaction with Naturally Reduced Ferruginous Smectite from a Redox Transition Zone. Environmental Science & amp; Technology, 2017, 51, 9042-9052.	4.6	38
42	Field Validation of Supercritical CO ₂ Reactivity with Basalts. Environmental Science and Technology Letters, 2017, 4, 6-10.	3.9	117
43	Ab initio thermodynamics of magnesium carbonates and hydrates in water-saturated supercritical CO2 and CO2-rich regions. Chemical Geology, 2016, 434, 1-11.	1.4	23
44	In Situ Natural Abundance ¹⁷ O and ²⁵ Mg NMR Investigation of Aqueous Mg(OH) ₂ Dissolution in the Presence of Supercritical CO ₂ . Environmental Science & Technology, 2016, 50, 12373-12384.	4.6	7
45	Size dependent microbial oxidation and reduction of magnetite nano- and micro-particles. Scientific Reports, 2016, 6, 30969. Heterogeneous growth of cadmium and cobalt carbonate phases at the <mml:math< td=""><td>1.6</td><td>34</td></mml:math<>	1.6	34
46	xmlns:mml="http://www.w3.org/1998/Math/MathML" altimg="si1.gif" overflow="scroll"> <mml:mfenced open="(" close=")"><mml:mrow><mml:mn>10</mml:mn><mml:mover accent="true"><mml:mn>1</mml:mn><mml:mo stretchy="true">Å⁻<mml:mn>4</mml:mn></mml:mo </mml:mover </mml:mrow></mml:mfenced 	1.4	18
47	calcite surface. Chemical Geology, 2015, 397, 24-36. Enhancing magnesite formation at low temperature and high CO2 pressure: The impact of seed crystals and minor components. Chemical Geology, 2015, 395, 119-125.	1.4	16
48	Evidence for Carbonate Surface Complexation during Forsterite Carbonation in Wet Supercritical Carbon Dioxide. Langmuir, 2015, 31, 7533-7543.	1.6	47
49	Uranium Redistribution Due to Water Table Fluctuations in Sandy Wetland Mesocosms. Environmental Science & Technology, 2015, 49, 12214-12222.	4.6	11
50	Dynamics of Magnesite Formation at Low Temperature and High pCO ₂ in Aqueous Solution. Environmental Science & Technology, 2015, 49, 10736-10744.	4.6	25
51	Formation of submicron magnesite during reaction of natural forsterite in H2O-saturated supercritical CO2. Geochimica Et Cosmochimica Acta, 2014, 134, 197-209.	1.6	36
52	CO ₂ Sorption to Subsingle Hydration Layer Montmorillonite Clay Studied by Excess Sorption and Neutron Diffraction Measurements. Environmental Science & Technology, 2013, 47, 205-211.	4.6	96
53	In Situ Spectrophotometric Determination of pH under Geologic CO ₂ Sequestration Conditions: Method Development and Application. Environmental Science & Technology, 2013, 47, 63-70.	4.6	20
54	Fayalite dissolution and siderite formation in water-saturated supercritical CO2. Chemical Geology, 2012, 332-333, 124-135.	1.4	51

#	Article	IF	CITATIONS
55	<i>In Situ</i> Molecular Spectroscopic Evidence for CO ₂ Intercalation into Montmorillonite in Supercritical Carbon Dioxide. Langmuir, 2012, 28, 7125-7128.	1.6	117
56	Controls on Soluble Pu Concentrations in PuO ₂ /Magnetite Suspensions. Environmental Science & Technology, 2012, 46, 11610-11617.	4.6	7
57	Reaction of water-saturated supercritical CO2 with forsterite: Evidence for magnesite formation at low temperatures. Geochimica Et Cosmochimica Acta, 2012, 91, 271-282.	1.6	97
58	In Situ X-ray Diffraction Study of Na ⁺ Saturated Montmorillonite Exposed to Variably Wet Super Critical CO ₂ . Environmental Science & Technology, 2012, 46, 4241-4248.	4.6	89
59	The Effect of pH and Time on the Extractability and Speciation of Uranium(VI) Sorbed to SiO ₂ . Environmental Science & Technology, 2012, 46, 6604-6611.	4.6	38
60	Heterogeneous Reduction of PuO ₂ with Fe(II): Importance of the Fe(III) Reaction Product. Environmental Science & Technology, 2011, 45, 3952-3958.	4.6	38
61	Impact of Particle Generation Method on the Apparent Hygroscopicity of Insoluble Mineral Particles. Aerosol Science and Technology, 2010, 44, 830-846.	1.5	44
62	Thermodynamic Model for the Solubility of TcO2â‹xH2O in Aqueous Oxalate Systems. Journal of Solution Chemistry, 2008, 37, 1471-1487.	0.6	12
63	Fe-solid phase transformations under highly basic conditions. Applied Geochemistry, 2007, 22, 2054-2064.	1.4	8
64	Development of Accurate Chemical Equilibrium Models for Oxalate Species to High Ionic Strength in the System: Na—Ba—Ca—Mn—Sr—Cl—NO3—PO4—SO4—H2O at 25 °C. Journal of Solution Che 2007, 36, 81-95.	em iste ry,	15
65	A Potentiometric, Spectrophotometric and Pitzer Ion-Interaction Study of Reaction Equilibria in the Aqueous H+-Al3+, H+-Oxalate and H+-Al3+-Oxalate Systems up to 5 molâ‹dmâ^'3 NaCl. Journal of Solution Chemistry, 2007, 36, 1727-1743.	0.6	12
66	Cancrinite and sodalite formation in the presence of cesium, potassium, magnesium, calcium and strontium in Hanford tank waste simulants. Applied Geochemistry, 2006, 21, 2049-2063.	1.4	50
67	Fluorescence spectroscopy of U(VI)-silicates and U(VI)-contaminated Hanford sediment. Geochimica Et Cosmochimica Acta, 2005, 69, 1391-1403.	1.6	136
68	An Aqueous Thermodynamic Model for the Complexation of Nickel with EDTA Valid to High Base Concentration. Journal of Solution Chemistry, 2004, 33, 1161-1180.	0.6	12
69	Dissolution of uranyl microprecipitates in subsurface sediments at Hanford Site, USA. Geochimica Et Cosmochimica Acta, 2004, 68, 4519-4537.	1.6	110
70	Chromium speciation and mobility in a high level nuclear waste vadose zone plume. Geochimica Et Cosmochimica Acta, 2004, 68, 13-30.	1.6	103
71	Title is missing!. Journal of Solution Chemistry, 2003, 32, 301-318.	0.6	2
72	Effect of Temperature on Cs+Sorption and Desorption in Subsurface Sediments at the Hanford Site, U.S.A Environmental Science & Technology, 2003, 37, 2640-2645.	4.6	66

#	Article	IF	CITATIONS
73	Selective Interactions of Soil Organic Matter Compounds with Calcite and the Role of Aqueous Ca. ACS Earth and Space Chemistry, 0, , .	1.2	4
74	Atom probe tomography and transmission electron microscopy: a powerful combination to characterize the speciation and distribution of Cu in organic matter. Environmental Sciences: Processes and Impacts, 0, , .	1.7	1